Macromolecular Research, Vol. 24, No. 1, pp 14-24 (2016)
DOI 10.1007/s13233-016-4001-0

www.springer.com/13233
pISSN 1598-5032 eISSN 2092-7673

In Situ Reactive Compatibilization of PP/ABS Blends *via* Friedel-Crafts Alkylation Reaction

Parvaneh Eskandari[1,2], Majid Mehrabi Mazidi[1,2], and Mir Karim Razavi Aghjeh*[,1,2]

[1]*Institute of Polymeric Materials, Sahand University of Technology, P.C:51335-1996, Tabriz, Iran*
[2]*Faculty of Polymer Engineering, Sahand University of Technology, P.C:51335-1996, Tabriz, Iran*

Received May 24, 2015; Revised October 13, 2015; Accepted October 15, 2015

Abstract: Friedel-Crafts alkylation reaction was employed to reactively compatibilize the polypropylene (PP)/acrylonitrile-butadiene-styrene (ABS) blends, using $AlCl_3$ as a catalyst. Rheology, morphology and mechanical properties of the reactive compatibilized blends along with the reference un-compatibilized samples were studied. Scanning electron microscopy (SEM) observations showed that blends containing catalyst exhibited an improvement in the dispersion state of ABS rubber particles. The results of mechanical tests revealed that reactive compatibilization partly increased the ultimate strength and Izod impact strength of the blends with a loss in tensile ductility. The change in these properties was explained in terms of different chemical reactions including grafting and degradation. Occurrence of these reactions was confirmed using different viscoelastic properties of the compatibilized blend samples. A great improvement in ultimate strength and impact toughness to levels much higher than those of neat PP was achieved in reactively compatibilized PP/ABS blends containing PP-*g*-MA. These findings were justified by morphological and rheological analyses. The formation of graft copolymer was also confirmed using Fourier transform infrared spectroscopy (FTIR) measurements. The results of impact toughness data were in agreement with the interfacial tension values measured *via* contact angle analysis. The deformation behavior of the different compatibilized samples was rationalized *via* fractographic study of the impact-fractured surfaces.

Keywords: polypropylene, rubber toughening, *in situ* compatibilization, friedel- crafts alkylation, mechanical properties.

Introduction

Isotactic polypropylene (PP) is the most widely used commodity thermoplastic with very large consumption because of its attractive properties such as low cost, good mechanical properties, excellent chemical and moisture resistance and easy processing and recycling.[1-4] However, the application of PP as a structural material is restricted due to its poor impact resistance, especially at low temperatures and notched trials.[5] It is well-known that the impact toughness of PP can greatly be improved by addition of elastomers such as ethylene-propylene rubber (EPR), ethylene-propylene-diene terpolymer (EPDM) and styrene-ethylene-butylene-styrene (SEBS) triblock copolymers as a secondary discrete phase.[6-11] It has well been established that the extent of improvement in impact strength of rubber-toughened thermoplastics would depend on the rubber type, its concentration, particle size and size distribution, and the level of interfacial adhesion with the surrounding matrix material.[12-17]

Acrylonitrile-butadiene-styrene (ABS) terpolymers, prepared by emulsion polymerization processes, are extensively used as impact modifier for styrenic polymers.[18,19] In contrast to above mentioned SBS and SEBS triblock copolymers, the ABS rubber particles have core-shell microstructure in which polybutadiene as a core phase is covalently grafted with styrene-acrylonitrile (SAN) copolymer as a shell during the polymerization process. The presence of such a shell provides good interfacial interaction with the styrenic matrices, leading to fine and uniform dispersion of the ABS toughener particles in the matrix with high toughening efficiency. To the best of our knowledge, few works have been performed in the field of PP/ABS blends.[20-23] Impact modification effect of ABS on PP with low impact resistance has not also been investigated. This may be due to the microstructure of ABS which makes it incompatible with PP, in contrast with olefinic modifiers commonly used as toughener for PP. In addition to its rubbery nature, it seems that the size of ABS particles (0.1 to 0.7 μm) is in the optimum size range reported for iPP matrix in order to achieve a high degree of rubber toughening. This was another reason which stimulated us to evaluate the phase structure and mechanical properties of PP/ABS blends.

The block or graft copolymers are frequently used as compatibilizing agents in immiscible polymer blends.[24-26] However, the reactive compatibilization is more desirable from both

*Corresponding Author. E-mail: karimrazavi@sut.ac.ir

the economic and academic points of view. This is because in this method the compatibilizer is *in situ* formed during the blending process and resides at the interfacial region between the blend components.[27] Due to the lack of special functional groups in the structure of polyolefins and styrenic polymers, some reactive species have been utilized for reactive compatibilization of polyolefins/styrenic polymers blends.[28,29] Freidel-Crafts alkylation reaction is another method for in-situ compatibilization of blends made of polyolefins and styrenic polymers.[28,29] In this method a halogenated alkane or olefin is chemically attached to the aromatic ring of styerene in the presence of a lewis acid. Carrick[30] synthesized a copolymer of PE and PS using $AlCl_3$ as an F-C alkylation reaction catalyst in a solution. Similarly, Heikens *et al*.[31,32] prepared a PE-*g*-PS copolymer for PE/PS blends and observed improvements in both morphology and mechanical properties. Baker *et al*.[33,34] have found that $AlCl_3$ has the highest reaction efficiency among all the studied Lewis acids. Gao *et al*.[35] used $AlCl_3$ to compatibilize LLDPE/PS and LLDPE/HIPS blends and evaluated the graft copolymer structure and stated that polyethylene chains were grafted to the para-position of the benzene rings of PS.

The present work was aimed to study the toughening efficiency of ABS rubber aggregation for iPP by *in situ* compatibilization of PP/ABS blends *via* Friedel-Crafts (F-C) alkylation reactions in the presence of $AlCl_3$. The effect of F-C reaction, on the phase morphology, melt rheology and mechanical properties was investigated. The results of compatibilization with F-C reactions were compared with those of physical blends compatibilized with maleic anhydride-grafted polypropylene (PP-*g*-MA) as a physical interfacial agent. Effect of PP-*g*-MA on the efficiency of the F-C reactions was also discussed.

Experimental

Materials. The polymers used in this study were obtained from commercial sources. Isotactic PP with a density of 0.9 g/cm^3 and melt flow index of 4.5 g/10 min was supplied by Polynar Corp., Tabriz, Iran. The ABS impact modifier with average particle size of 0.33 μm was provided by Tabriz Petrochemical Company, Iran. Other characteristics of ABS are given in Table I. Maleic-anhydride grafted polypropylene (PP-*g*-MA) with 0.8% MA as a physical compatibilizer with a density of 0.91 g/cm^3 and melt flow index of 80 g/10 min was supplied by Pluss Polymer Corp., India. The catalyst of Friedel-Crafts reaction was aluminum chloride ($AlCl_3$) (> 98% purity) from Merck. About 0.3 wt% styrene monomer (St) (>99.7% purity) was used as a cocatalyst.[36,37]

Table I. Characteristics of ABS Impact Modifier

PB/SAN (wt/wt)	St/AN (wt/wt)	PB/St/AN (wt/wt/wt)	Average Particle Size (nm)
56/44	72.5/27.5	56/32/12	330

Blend Preparation. The PP/ABS (80/20) and PP/PP-*g*-MA/ABS (75/5/20) physical blends and the reactive blends containing various amounts of $AlCl_3$ were prepared in a laboratory batch internal mixer (Brabender W50 EHT) at starting temperature of 170 °C with 60 rpm for 10 min. In the case of the reactive blends, the Friedel-Crafts reaction was performed after the steady-state torque was reached. The concentration of $AlCl_3$ was adjusted at 0.5, 0.7, and 1 wt% which were incorporated into mixing chamber at about 5 min from the beginning of the mixing process of the blend components. Reactive blends were prepared at the presence of 0.3 wt% styrene monomer as a cocatalyst.[36,37]

Rheological Studies. Rheological properties of the pure components together with physical and reactive blends were determined using a dynamic rheometer (MCR301, Anton Paar) equipped with parallel plate geometry (diameter=25 mm, gap =1 mm). The frequency sweep tests from 0.04 to 625 rad/s was performed at 200 °C under dry nitrogen atmosphere, with amplitude of 1% in order to maintain the response of the materials within the linear viscoelastic regime.

Morphological Observations. A small amount of the prepared blend samples was rapidly quenched in liquid nitrogen for morphological study and then the cryo-fractured surfaces were etched with THF (tetrahydrofuran) for 24 h at 50 °C for the removal of ABS phase. In addition to the internal morphology of different samples, the characteristics of the impact-fractured surfaces obtained after Izod impact tests was also studied. The surfaces of the samples were gold sputtered for good conductivity of the electron beam. Morphology of the prepared samples was examined using scanning electron microscopy (SEM, LEO 440 I, UK).

Mechanical Properties. The tensile properties of the dumb bell-shaped samples were evaluated in a Zwick/Roell tensile testing machine (Z010) according to ASTM D-638 at a strain rate of 50 mm/min. At least five specimens were tested for each sample at room temperature and the results were averaged. Notched Izod impact strength of the samples was measured on a GOTECH impact testing machine (GT 7045) according to the ASTM D-256 standard. At least five specimens for each composition were tested at room temperature and the results were averaged.

Fourier Transform Infrared Spectroscopy (FTIR). FTIR analysis was performed to evaluate the formation of the copolymer in the reactive compatibilized blends. Before the FTIR analysis the samples were grinded and extracted with boiling xylene to remove the ungrafted PP chains. The remained material (rubber particles and the grafted PP chains on their surfaces) was dried in a vacuum oven and then molded into thin films (15-20 μm) in a hot press at 190 °C. FTIR spectra were taken using a FTIR spectrometer (Bruker Tensor 27) at resolution of 0.5 cm^{-1}.

Contact Angle Measurements. Contact angles of different samples were measured in a sessile drop mold with KRUSS DSA100 (Germany). Neat polymers and the blends were com-

pression-molded between clean silicon wafers at 190 °C for 5 min and then cooled to 30 °C. Contact angles were measured on 3 mL of wetting solvent at 25 °C, and the mean values of five replicates were reported.

Results and Discussion

Chemical Aspects. In this work, F-C alkylation reaction was carried out on PP/ABS blends to generate compatibilizing graft copolymers. A general scheme for the formation of grafted copolymer *via* F-C alkylation reaction can be given as Scheme I in Figure 1.[38]

Benzene ring of polystyrene is susceptible to electrophilic attack primarily because of its exposed π electrons. The reaction occurs in three steps: 1) A carbocation is formed by reaction of a halogenated alkane with aluminum chloride; 2) the carbocation (acting as an electrophile) hits the benzene ring to form an arenium ion; and 3) the arenium ion loses a proton to produce the alkylated benzene. A general scheme of benzene ring acylation in the presence of maleic anhydride groups and formation of grafted copolymer is given in Scheme II in Figure 1.[39]

As can be seen, the acylation reaction consists of several stages: 1) Complex formation of MA groups with Lewis acid (MX_n); 2) addition of the complex to the phenyl ring of PS and 3) break of the hydrogen atom from the *p*- or *o*-position of phenyl ring and its addition to maleated fragment.

Dynamic Rheology. The changes of complex viscosity (η^*) and storage modulus (G') as functions of angular frequency (ω) for pure PP, pure ABS and PP/ABS (80/20) blend are shown in Figure 2.

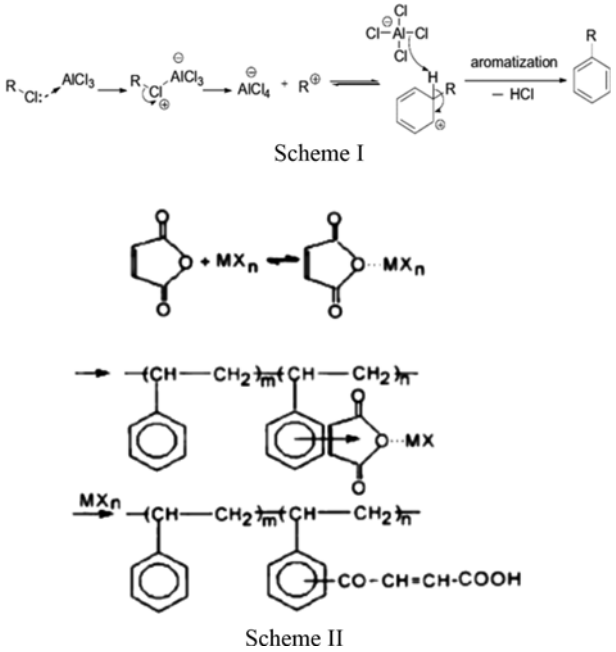

Figure 1. A general scheme of benzene ring acylation and alkylation.

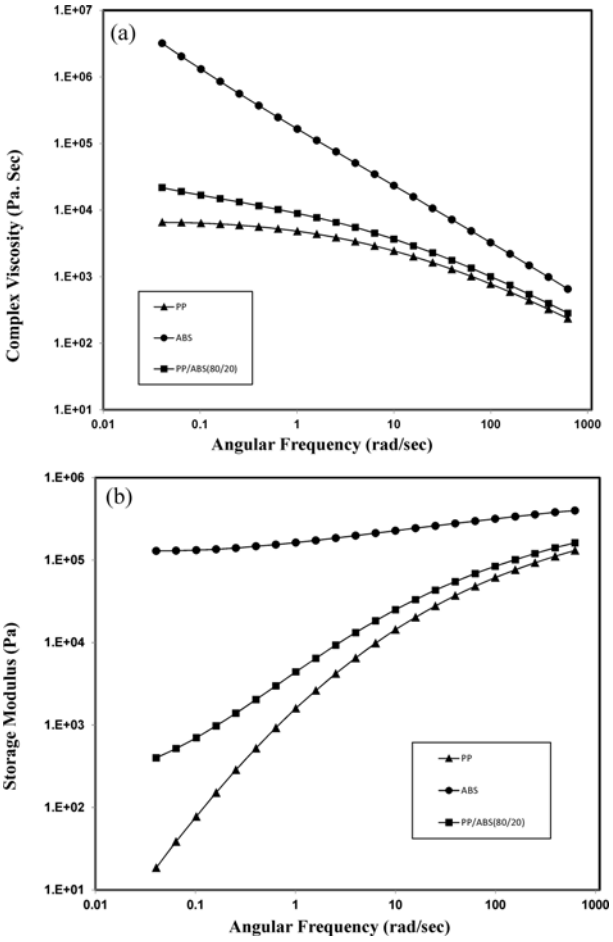

Figure 2. The results of (a) complex viscosity (η^*) and (b) storage modulus (G') *vs*. angular frequency for neat components and PP/ABS (80/20) blend.

As shown, both polymers (PP and ABS) display power-law behavior with shear-thinning response, and ABS exhibits higher viscosity and elasticity than the PP over the entire range of angular frequency. The difference in viscoelastic behavior of PP and ABS becomes more pronounced as the angular frequency was reduced. While the neat PP relaxes at low frequencies, the ABS terpolymer shows a non-terminal response even at very low frequencies due to its elastomeric nature. The addition of 20 wt% of ABS terpolymer into PP increased the complex viscosity of the material especially at low frequency region, so that the PP/ABS (80/20) blend showed a slight upturn at low-frequency zone. In the case of melt elasticity, the PP/ABS blend exhibits a significant increase in storage modulus as compared to neat PP so that a plateau observed at low frequencies, indicating the formation of a solid-like structure in the blend.

It is well-known that the dynamic viscoelastic properties of polymer blends are strongly dependent on the interfacial interactions. In fact, the viscoelastic response of the multiphase systems at low frequencies reflects the phase morphology

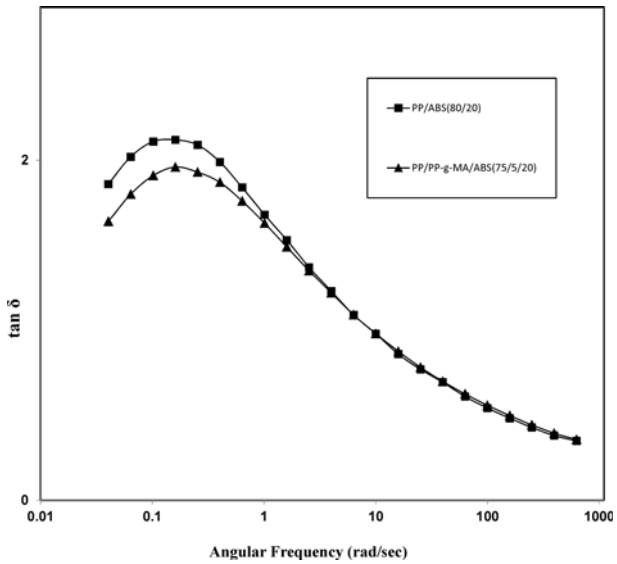

Figure 3. Loss tangent (tan δ) *vs.* angular frequency of uncompatibilized and physically compatibilized PP/ABS (80/20) blends.

and dispersion state of components.[40-42]

The appearance of a solid-like behavior at low frequencies for PP/ABS (80/20) blend may be attributed to the formation of aggregated structures of ABS rubber particles in the PP matrix having high interfacial tension with the surrounding matrix material. However, the rubbery nature of ABS aggregation of high elasticity may partly contribute to this type of response.

Figure 3 shows the frequency dependence of damping factor (tan δ) for uncompatibilized and physically compatibilized PP/ABS (80/20) blend using 5 wt% PP-*g*-MA. As can be seen, the loss tangent of compatibilized blend (PP/PP-*g*-MA/ABS (75/5/20)) is lower than that of uncompatibilized blend (PP/ABS (80/20)) at low frequency regions, where the loss tangent response can be used for evaluating of the interfacial interaction between phases. This alteration in loss tangent response could be ascribed to compatibilizing effect of PP-*g*-MA in PP/ABS blends.

The effect of $AlCl_3$ on the dynamic viscoelastic properties of neat PP and ABS phase is depicted in Figure 4. From the results, it is clear that the addition of 0.5 wt% of $AlCl_3$ reduced the melt viscosity of PP (from 1.27×10^4 to 1.08×10^4 Pa·s @ ω=0.04 rad/s) and its elasticity (from 2.09×10^5 to 1.7×10^5 Pa @ ω=625 rad/s). Nearly, the same effect was observed upon the introduction of $AlCl_3$ into ABS terpolymer, but with lower intensity (modulus from 3.98×10^5 to 3.89×10^5 Pa @ ω=625 rad/s). It is believed that the degradation of both PP and ABS followed by reduction in their molecular weight *via* chain-scission reaction is responsible for lowered viscoelastic properties of the neat PP and ABS phases upon the addition of $AlCl_3$.

The effect of $AlCl_3$ content on the melt elasticity and damping capacity of PP/ABS (80/20) blend is shown in Figure 5. As can be seen in Figure 5(a) the blends incorporated with different concentrations of $AlCl_3$ (0.5, 0.7, and 1.0 wt%) showed higher storage modulus values at low frequencies as compared with the uncompatibilized blend. This type of behavior can be seen in compatibilized systems with improved interfacial interactions.

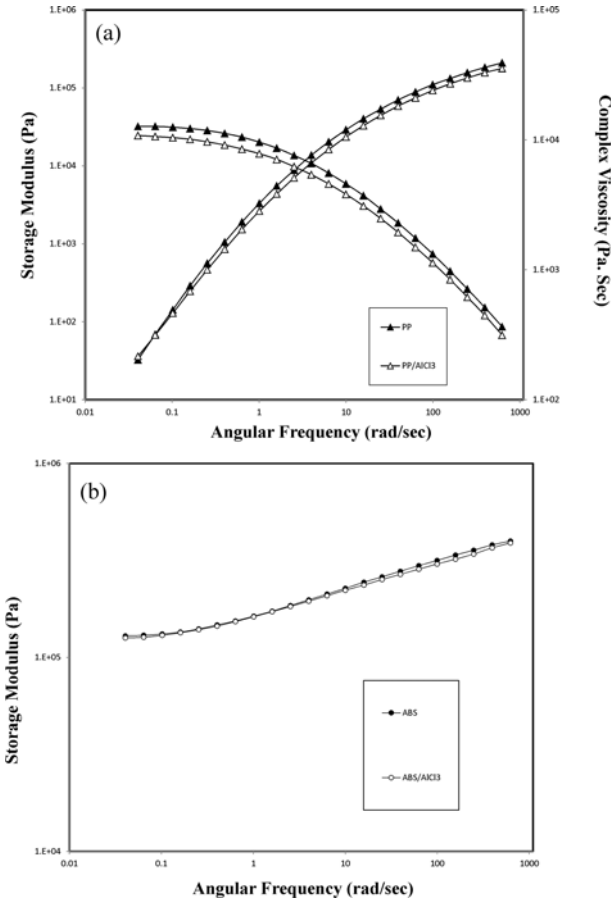

Figure 4. Effect of $AlCl_3$ on the viscoelastic properties of (a) PP homopolymer and of (b) ABS terpolymer.

The improved interfacial interactions between the dispersed phase and the matrix upon the addition of different amount of $AlCl_3$ can be related to the *in situ* formation of PP-*g*-SAN copolymer which acts as compatibilizing agent in the PP/ABS blend. A general scheme for the PP-*g*-SAN formation *via* F-C alkylation reaction is presented in Figure 6.

The *in situ* formed PP-*g*-SAN at the interfacial region between PP and ABS phase can reduce the interfacial tension and increase the interfacial adhesion. As a result, the macromolecular movement and chain slippage at the interfacial region between the components becomes restricted, which manifests itself as increased melt elasticity. Nevertheless, the reactive system containing 1.0 wt% of $AlCl_3$ exhibits a reduction in elastic response at intermediate to high frequency ranges compared to other blends. This indicates that the addition of 1.0 wt%

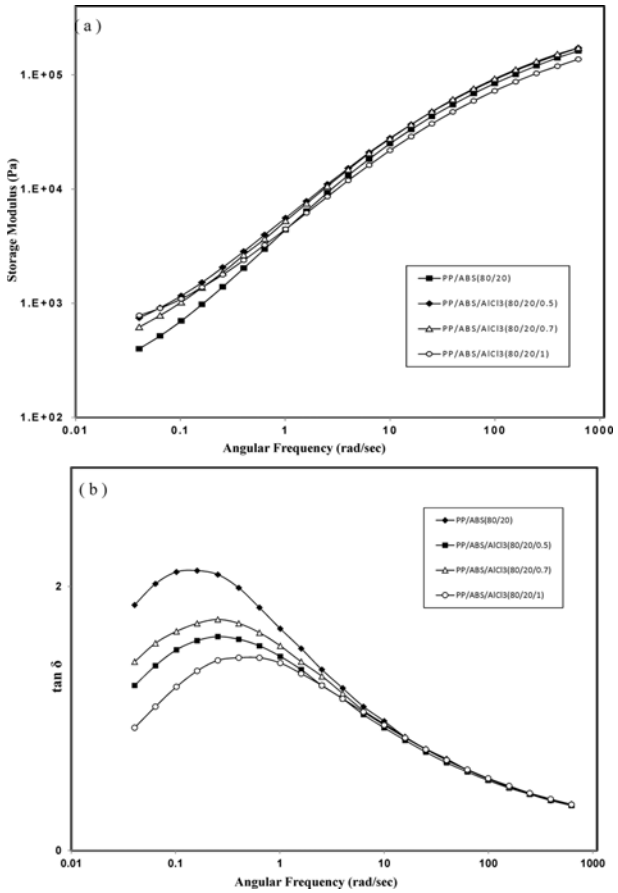

Figure 5. Effect of $AlCl_3$ concentration on the (a) storage modulus and (b) tan δ of PP/ABS (80/20) blend.

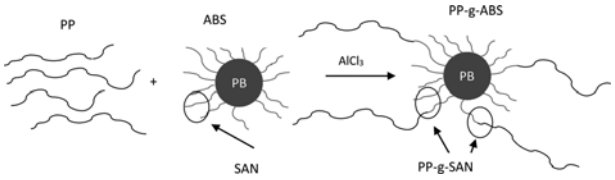

Figure 6. A representative scheme for the compatibilizer copolymer formation.

although improves the interfacial interaction between the dispersed phase and the matrix, but causes some degradation through chain scission reactions of matrix material.

According to Figure 5(b), the $AlCl_3$ concentration mainly affects the damping factor of PP/ABS blend at low frequency regions, where the interfacial interactions between the components controls the viscoelastic response. The damping capability of the different reactive blends is much lower than that of uncompatibilized blend, which is in agreement of the storage modulus variation. As stated above, the *in situ* formation of PP-*g*-SAN copolymer enhances the intermolecular interaction at the interface between PP and ABS components, which in turn, severely impedes the chain mobility and relaxation processes at the interfacial region. Therefore the inner loss of the material will reduce causing a substantial reduction in damping capacity of the reactively compatibilized blends.

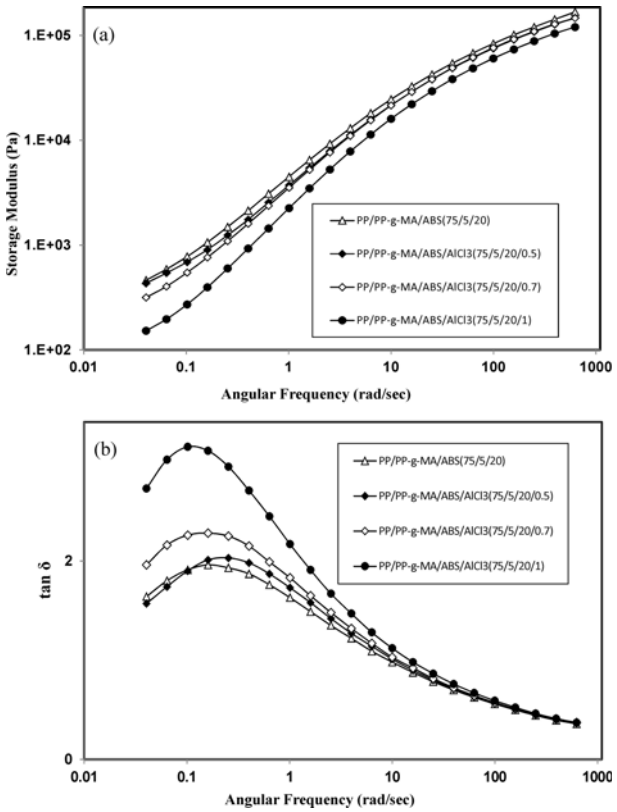

Figure 7. (a) Storage modulus and (b) loss tangent of PP/PP-*g*-MA/ABS (75/5/20) blend containing various amounts of $AlCl_3$ catalyst.

PP/PP-*g*-MA/ABS (75/5/20) blends were prepared with various amounts of $AlCl_3$ to the following reasons; The first reason was the fact that PP-*g*-MA can affect the compatibility of the system, which was indicated in Figure 3 and reported in other research works.[23] The second reason for introduction of PP-*g*-MA into PP as matrix was to prevent PP from degradation by $AlCl_3$. Simultaneous presence of $AlCl_3$ and PP-*g*-MA in PP system can extend the PP chains leading to enhancing in matrix viscosity, which may decrease the aggregation of ABS domains. The tendency of maleic anhydride groups to F-C acylation reaction in the presence of $AlCl_3$ was the last reason. In this situation both the F-C acylation and alkylation reactions can simultaneously operate, leading to increase in the amount of compatibilizer at the interface. This can also lead to an improvement in dispersion state of rubber particles by reduction of interfacial tension. As can be seen from the Figure 7, by adding $AlCl_3$, the storage modulus of the blends decreased. This reduction may be related to the dispersion of aggregated ABS domains, which seems dominates the effect of increased interfacial interaction. Improving of the dispersion state would increase the damping factor (Figure 7(b)).

Phase Morphology. Figure 8 shows the SEM images of cryogenically fractured surfaces of PP/ABS blend without

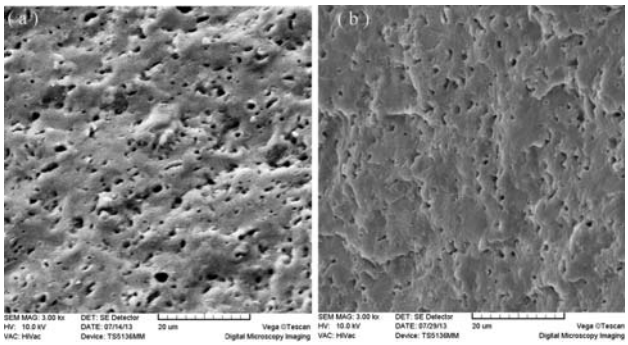

Figure 8. The SEM micrographs of cryogenically fractured surface of blends: (a) PP/ABS (80/20) and (b) PP/PP-*g*-MA/ABS (75/5/20).

and with 5 wt% PP-*g*-MA. The cavities on the surfaces correspond to the location of ABS dispersed phase, which was selectively removed by THF solvent. It is important to note that the holes on the surfaces are due to the aggregates of ABS particles because the size of the holes is much larger than that of ABS primary particles (430 nm). As can be seen, the morphology of the blends is matrix-dispersed type. It is also observed that the addition of PP-*g*-MA into PP/ABS (80/20) improved the dispersion of aggregated ABS domains in the matrix *via* a reduction of the number average diameter from 1.6 μm (Figure 8(a)) to 1.22 μm (Figure 8(b)). This indicates that PP-*g*-MA acts as a compatibilizer in PP/ABS blends. As an emulsifying agent, PP-*g*-MA reduces the interfacial tension between the PP and ABS phases, giving rise to a finer dispersion of ABS aggregates in the PP matrix.

Figure 9 shows the SEM micrographs of reactive PP/ABS blends containing various amounts of $AlCl_3$. Figure 9(b) shows larger and coarsely dispersed cavities with the number average diameter of about 3 μm. As can be seen aggregated ABS domains size get increased after 0.5 wt% of $AlCl_3$ addition which could result from the decreased matrix viscosity. This has dominated to the effect of increased interfacial interaction, which basically improves the dispersion of aggregates. Due to sufficient amount of PP-*g*-SAN copolymer and compatibilization effect, aggregated ABS domains size get smaller with the number average diameter of about 2 μm in PP/ABS/$AlCl_3$ (80/20/0.7) blend compared to that of PP/ABS/$AlCl_3$ (80/20/0.5) blend with the number average diameter of about 3 μm (Figure 9(c)). As it mentioned before, disaggregate of PP/ABS/$AlCl_3$ (80/20/1) is obvious in Figure 9(d).

The SEM micrographs of cryogenically fractured surfaces of PP/PP-*g*-MA/ABS (75/5/20) blends containing 0, 0.5, 0.7, and 1.0 wt% of $AlCl_3$ are shown in Figure 10. The main point of these SEM micrographs is the dispersion improvement after adding $AlCl_3$ into the blends. These results confirm that using $AlCl_3$ in the blends containing PP-*g*-MA, appreciably improves the interfacial interaction leading to better stress transfer from the PP matrix to the segregated ABS domains, which finally results in better dispersion of the rubber particles. Dispersion improvement is the reason why the melt elasticity at low frequency ranges decreases after $AlCl_3$ addition (Figure 10).

The presence of 0.5 wt% of $AlCl_3$ reduced the number average diameter of aggregated ABS domains to 1.2 μm (Figure

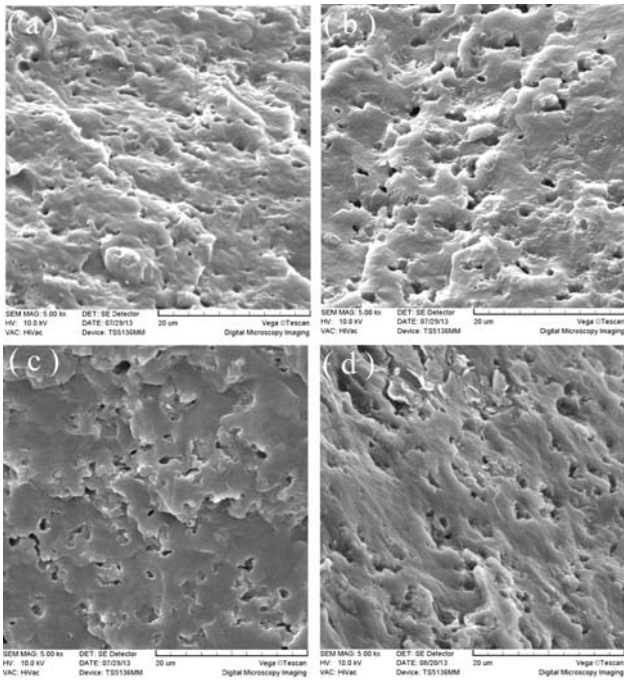

Figure 9. SEM micrographs taken from cryogenically fractured surface of PP/ABS (80/20) uncompatibilized blend and compatibilized with various amounts of $AlCl_3$: (a) 0 wt%, (b) 0.5 wt%, (c) 0.7 wt%, and (d) 1 wt%.

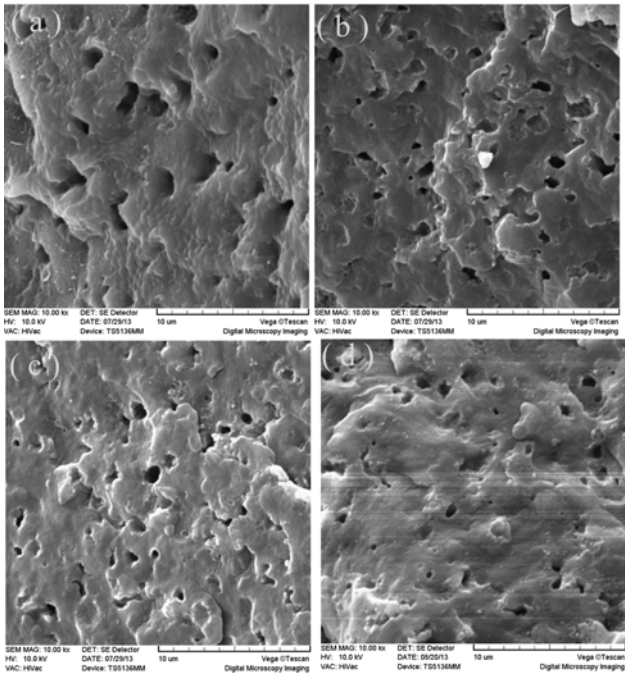

Figure 10. SEM micrographs taken from cryogenically fractured surface of PP/PP-*g*-MA/ABS (75/5/20) blends with various amounts of $AlCl_3$: (a) 0 wt%, (b) 0.5 wt%, (c) 0.7 wt%, and (d) 1 wt%.

10(b)). In addition, some dispersed ABS aggregations still have the size in the range of that for blend without $AlCl_3$.

By reaching $AlCl_3$ amount to 0.7 wt%, dispersion improved with further decrease in the number average diameter of dispersed ABS domains to 1 μm (Figure 10(c)). It is probably due to the formation of sufficient amount of compatibilizer at the interface *via* F-C acylation and alkylation reactions, which lead to the reduction of interfacial tension between the dispersed ABS aggregates and the matrix. Further increase in the $AlCl_3$ concentration resulted in a reduction of aggregated ABS domains either, 0.45 μm, by formation of copolymer or by disaggregation of ABS phases (Figure 10(d)).

Mechanical Properties. Figure 11 shows the ultimate tensile properties and impact strength of neat PP and PP/ABS (80/20) blends with different amounts of $AlCl_3$. The elongation at break of the PP increased after addition of ABS (Figure 11(a)) while its tensile strength decreased (Figure 11(b)).

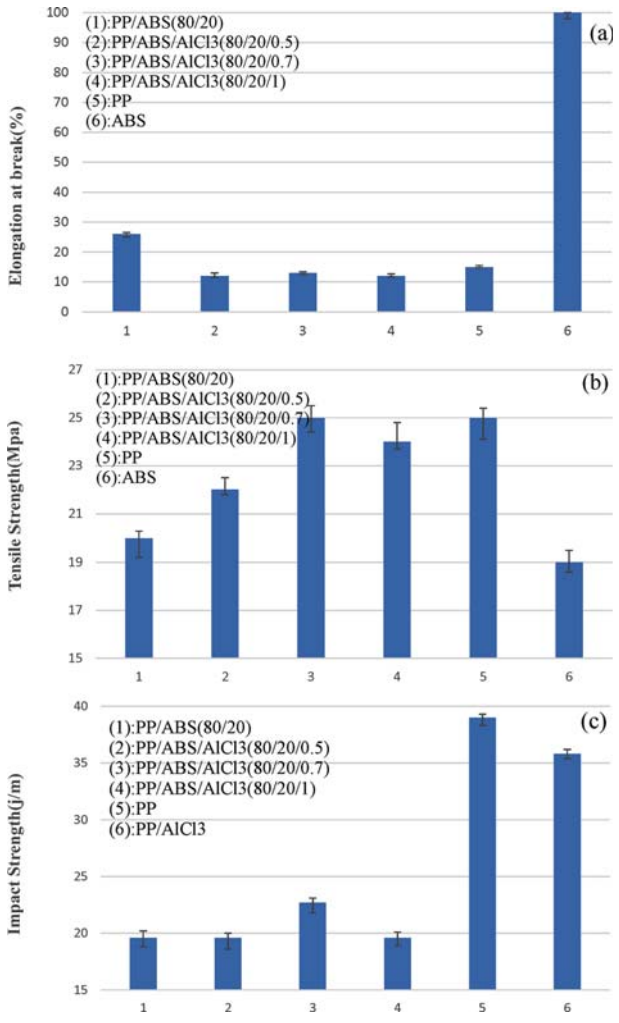

Figure 11. Mechanical properties of PP/ABS (80/20) with various amount of $AlCl_3$ in compared with PP: (a) Elongation at break, (b) tensile strength, and (c) impact strength of PP/ABS (80/20) with various amount of $AlCl_3$ in compared with PP and PP/$AlCl_3$.

The former is because of rubber toughening effect of ABS, which has high elongation at break and low tensile strength, in the PP/ABS blend and the latter is due to the week interfacial adhesion between PP and ABS.

The addition of $AlCl_3$ to PP/ABS blend in different levels greatly reduced the elongation at break. The decrease of the elongation at break in blends by adding various amounts of $AlCl_3$ may be due to the fact that the elongation at break is sensitive to the chain scission reactions induced by $AlCl_3$. On the other hand, tensile strength is related to the morphology, domain size and dispersion state of the minor component in the multiphase system, which may be regarded as a measure of interfacial strength between the components. As can be seen in the Figure 11(b), the addition of 0.5 and 0.7 wt% of $AlCl_3$ gradually increased the tensile strength, while a little decrease was observed for the blend containing 1.0 wt% of $AlCl_3$, but is still much higher than that of uncompatibilized PP/ABS blend. A significant improve in tensile strength of the reactive PP/ABS (80/20) blends of different amounts of $AlCl_3$, which indicates to the much higher load-bearing capability of the blend, could be attributed to the enhanced interfacial adhesion between different components caused by *in situ* formation of PP-*g*-SAN graft copolymer *via* F-C alkylation reaction. In fact, the *in situ* generated copolymer provides strong phase adhesion between the components following by efficient stress transfer through the interfacial region, leading to improved load-bearing capacity of the reactively compatibilized blend. The notched impact strength of neat PP, PP/$AlCl_3$, and reactive PP/ABS (80/20) blends containing different amounts of $AlCl_3$ is depicted in Figure 11(c). While the ABS polymer showed very high impact strength value (237 j/m), its incorporation into PP reduced the impact resistance of the material because of poor interfacial bonding in the PP/ABS blend. The decrease of impact strength of PP after $AlCl_3$ addition may be due to the reduction in molecular weight *via* chain scission reactions. Among the reactive blends with different $AlCl_3$ contents, the blend containing 0.7 wt% of $AlCl_3$ showed the higher impact strength. However, the impact strength of this blend is much lower than that of pure PP and PP/$AlCl_3$.

As stated before, the *in situ* compatibilization through the F-C alkylation reaction involves the occurrence of chain scission reactions followed by the process of graft copolymer formation. Therefore both degradation and copolymer formation processes concurrently occur upon the addition of $AlCl_3$ into the blend to be compatibilized. The prevalent process in the melt mixed blend depends on the concentration of $AlCl_3$ and the blend composition as well. It is well established that there is a critical concentration of $AlCl_3$, above which the molecular degradation processes in the form of chain scission reactions becomes more predominant. Below this concentration the copolymer formation reactions are dominant over chain scission reactions and good properties are ensured. According to the mechanical properties presented in Figure 11, it was assumed that the 0.7 wt% of $AlCl_3$ is the critical concen-

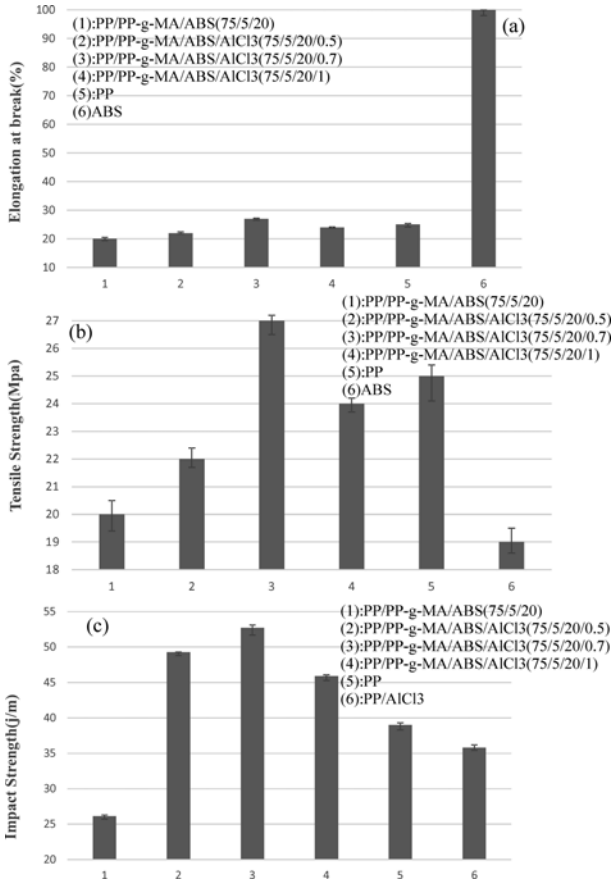

Figure 12. Mechanical properties of PP/PP-*g*-MA/ABS (75/5/20) with various amount of $AlCl_3$ in compared with PP: (a) Elongation at break, (b) tensile strength, and (c) impact strength of PP/PP-*g*-MA/ABS (75/5/20) with various amount of $AlCl_3$ in compared with PP and PP/$AlCl_3$.

tration in terms of morphological and mechanical results. However to verify the reality of such an assumption, molecular weight measurements should be applied. In this case because of crosslinked nature of rubbery phase molecular weight measurements are not applicable.

Figure 12 shows the effect of $AlCl_3$ content on the elongation at break, tensile strength and impact strength of the PP/PP-*g*-MA/ABS (75/5/20) blend. The reactive blends containing various amounts of $AlCl_3$ show slightly higher strain at break as compared with those of blends without $AlCl_3$ (Figure 12(a)). However, the reactive blend with 0.7 wt% of $AlCl_3$ exhibits the highest tensile extensibility among the reactive blends. The large decrease in the tensile toughness of the reactive blend with 1.0 wt% of $AlCl_3$ is due to intensive macromolecular degradation of the matrix material, which severely affects the tensile ductility of the blend.

In the case of tensile strength, it is obvious that the ultimate strength of the blends initially increased with $AlCl_3$ content and then decreased at higher loadings of $AlCl_3$ (Figure 12(b)). The tensile strength values of all the reactive blends are much higher than that of the blend without $AlCl_3$. Similar to the PP/ABS (80/20) blends described in Figure 11(b), the decrease in stress at break for the blend with 1.0 wt% of $AlCl_3$ could be ascribed with the higher degree of degradation reactions in this system compared to the reactive blends with lower $AlCl_3$ contents.

The impact strength values for PP/PP-*g*-MA/ABS (75/5/20) blends without and with different amounts of $AlCl_3$ are shown in Figure 12(c). The notched impact strength of the PP homopolymer and PP/$AlCl_3$ is also given as the reference materials. It is apparent that the impact resistance of PP/PP-*g*-MA/ABS (75/5/20) blend is lower than that of neat PP and PP/$AlCl_3$. Although PP-*g*-MA serves as a physical compatibilizer in this blend, the impact data indicate that rubber toughening effect is not achieved in the physically compatibilized PP/ABS blend. This may be due to not sufficient interfacial strength at the interface between the components, which could not shows load-bearing capability under impact condition. It is worth to note that the physically compatibilized PP/ABS blend showed higher impact strength value than its uncompatibilized counterpart, most likely due to higher interfacial interactions between the components in the former system, but not strong enough to display rubber toughening effect in the PP matrix.

The addition of different levels of $AlCl_3$ into PP/PP-*g*-MA/ABS (75/5/20) blend led to a pronounced increase in the impact resistance, so that the entire reactive blends showed much higher impact resistance value than that of reference PP and PP/$AlCl_3$. Among the reactive blends in Figure 12(c), the system reactively compatibilized with 0.7 wt% of $AlCl_3$ showed the highest impact resistance value. Further loading of $AlCl_3$ decreased the impact toughness of the material, but is still higher than that of pure PP and PP/$AlCl_3$.

It is important to note that the presence of PP-*g*-MA in the system may promote acylation reactions in addition to conventional alkylation reactions taking place in the reactive blends. Therefore, both processes participate in the strengthening of the interfacial area followed by much efficient stress transfer across the interfacial region between the components. As a result, the impact strength improves significantly. The micro-mechanisms of deformation under the impact loading conditions together with the toughening processes involved in the reactive blends is discussed in the fractography section.

Fractography. Figure 13 shows the SEM micrographs taken from impact fractured surfaces of PP/ABS blends without and with 0.7 wt% of $AlCl_3$. From the results, it is observed that the fractured surface of PP/ABS blend is rougher than that of the blend containing 0.7 wt% of $AlCl_3$. This shows that by addition of $AlCl_3$, reactive blend absorbs much more energy during the deformation processes. As mentioned above, in the presence of $AlCl_3$ the size of dispersed aggregates of ABS phase get larged by chain scission of the matrix.

Figure 14 depicts the SEM images of impact fractured surfaces of PP/PP-*g*-MA/ABS (75/5/20) and PP/PP-*g*-MA/ABS/

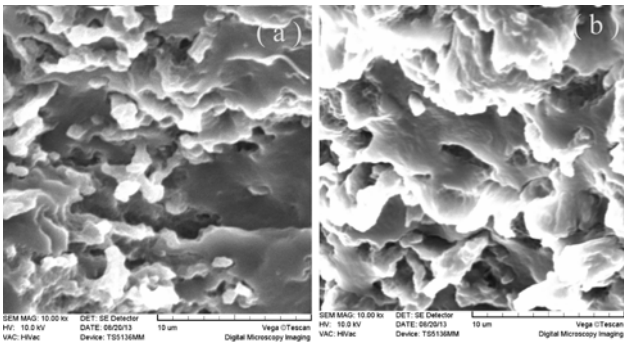

Figure 13. SEM micrographs taken from impact fractured surfaces of blends: (a) PP/ABS (80/20) and (b) PP/ABS/$AlCl_3$ (80/20/0.7).

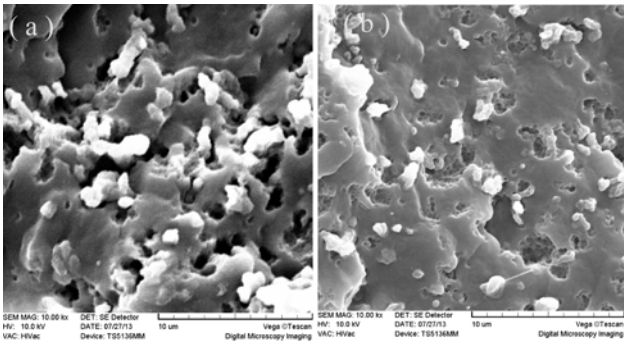

Figure 14. SEM micrographs taken from impact fractured surfaces of blends: (a) PP/PP-*g*-MA/ABS (75/5/20) and (b) PP/PP-*g*-MA/ABS/$AlCl_3$ (75/5/20/0.7).

$AlCl_3$ (75/5/80/0.7) blends. The fractured surface of physical blend shows that the ABS aggregates are deboned from the matrix material under the impact loadings. This indicates that the presence of PP-*g*-MA could not provide sufficient interfacial adhesion to resist against particles decohesion and the formation of critical-sized interfacial voids and micro-cracks.

In contrast, the reactively compatibilized blend with 0.7 wt% of $AlCl_3$ not only shows good dispersion of ABS particles in the matrix, but also exhibits sufficient interfacial bonding with surrounding matrix material which prevents early detachment of ABS clusters from the matrix under the impact loadings.

The improved interfacial adhesion in the reactive blends efficiently transfers the stress from the matrix to the ABS particles through the interfacial region which, in turn, led to higher load-bearing capability of the system. As a result, the material resistance against early crack initiation would be increased. In the case of reactively compatibilized blend in Figure 14(b), it should be noted that the interfacial adhesion between the components is not very strong. This is evidenced by the presence of strawberry-shaped cavities on the impact fracture surface, which are related to the detachment of dispersed aggregates of ABS particles. This intermediate level interfacial bonding is beneficial to dissipation of impact loadings. Because the process of stress transfer through the interfacial region followed by some debonding and/or detachment of dispersed

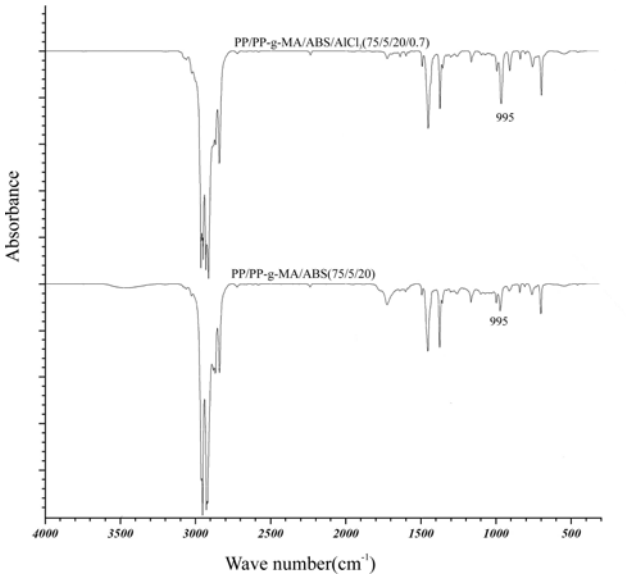

Figure 15. Fourier transform infrared spectra of the PP/PP-*g*-MA/ABS (75/5/20) and PP/PP-*g*-MA/ABS/$AlCl_3$ (75/5/20/0.7) samples.

rubbery domains plays a significant role in absorption and/or dissipation of impact energy. Although the reactive blend showed higher impact strength compared with non-reactive one, the fracture surface of both blends are smooth with no sign of stress whitening, which are characteristics of brittle mode of failure with unstable crack propagation.

Fourier Transform Infrared Spectroscopy. The infrared spectra of the PP/PP-*g*-MA/ABS (75/5/20) and PP/PP-*g*-MA/ABS/$AlCl_3$ (75/5/20/0.7) blends are shown in Figure 15.

The absorbance bands appearing at 520, 570, 1453, and 2243 cm^{-1} are related to acrylonitrile and those appearing at 540, 690, 1450, 1490, 1610, 2960, and 3070 cm^{-1} indicate the presence of styrene.[43] The absorbance bands occurring at 708, 916, 970, 1649, 2950, and 3070 cm^{-1} are related to polybutadiene. Further the absorbance bands which are appearing at 810, 842, 895, 974, 1045, 995, 1153, 1168, 1258, 1380, 1356, and 1465 cm^{-1} are corresponded to the polypropylene.[43]

The ratios of absorbance peaks at 1649, 1490, 1453, and 995 cm^{-1}, the characteristic peaks of polybutadiene, styrene, acrylonitrile and polypropylene respectively, were selected to indicate the presence of each component.

The analysis of the spectra shows that with the addition of $AlCl_3$ in presence of PP-*g*-MA, there is an increase in the intensity of the peaks of absorption located at 995 cm^{-1}, which correspond to the stretching of the PP. This can be related to PP chains grafted on the SAN chains to form compatibilizer copolymer. These observations support the suggestion of the formation of copolymer through the Friedel-Crafts reaction that was proposed as a main cause of change in phase morphology with subsequent improvement of impact strength of the blends.

Table II. Contact Angle and Surface Tension Results for Different Samples

Sample	Contact Angle (°)		Surface Tension (mN/m)		
	Water	Diiodomethane	Total (γ)	Dispersion Component (γ^d)	Polar Component (γ^p)
PP	108	49.2	45.84	44.2	1.64
ABS	45	53	55.2	22.2	33
PP-*g*-MA	79.5	45	49.85	47.35	2.5
PP/ABS	66.4	53.7	48.81	26.2	22.61
PP/ABS/$AlCl_3$	98	43.5	47.8	45.4	2.7
PP/PP-*g*-MA/ABS	101.6	47	51.7	47.5	4.2
PP/PP-*g*-MA/ABS/$AlCl_3$	108.5	52	52.69	48.19	4.5

Contact Angle Measurements. The results of morphological studies showed that the dispersion of ABS domains improved after adding PP-*g*-MA and 0.7 wt% $AlCl_3$. In this section an attempt was made to quantitatively evaluate the interfacial tension between the components and as affected by the presence of PP-*g*-MA and $AlCl_3$. The contact angles with water and diiodomethane for neat polymers and selected systems are summarized in Table II. From the contact angle data, the polar and dispersive components of surface tension were measured by following equations:[44]

$$(1+\cos\theta_{H_2O})\gamma_{H_2O} = 4\left(\frac{\gamma^d_{H_2O}\gamma^d}{\gamma^d_{H_2O}+\gamma^d}+\frac{\gamma^p_{H_2O}\gamma^p}{\gamma^p_{H_2O}+\gamma^p}\right) \quad (1a)$$

$$(1+\cos\theta_{CH_2I_2})\gamma_{CH_2I_2} = 4\left(\frac{\gamma^d_{CH_2I_2}\gamma^d}{\gamma^d_{CH_2I_2}+\gamma^d}+\frac{\gamma^p_{CH_2I_2}\gamma^p}{\gamma^p_{CH_2I_2}+\gamma^p}\right) \quad (1b)$$

In which $\gamma = \gamma^d + \gamma^p$, $\gamma_{H_2O} = \gamma^d_{H_2O} + \gamma^p_{H_2O}$, $\gamma_{CH_2I} = \gamma^d_{CH_2I} + \gamma^p_{CH_2I}$, γ is surface tension, *d* is dispersion component, and *p* is polar component, θ_{H_2O} and $\theta_{CH_2I_2}$ are contact angles of the samples with water and diiodomethane, respectively. The numerical values used are $\gamma^d_{H_2O} = 22.1$ (mN/m), $\gamma^p_{H_2O} = 50.7$ (mN/m), $\gamma^d_{CH_2I_2} = 44.1$ (mN/m), $\gamma^p_{CH_2I_2} = 6.7$ (mN/m). The values of surface tension, dispersion and polar components are also listed in Table II.

The interfacial tension between different polymers can be further calculated by the following equation:[44]

$$\gamma_{AB} = \gamma_A + \gamma_B - \frac{4\gamma^d_A\gamma^d_B}{\gamma^d_A+\gamma^d_A} - \frac{4\gamma^p_A\gamma^p_B}{\gamma^p_A+\gamma^p_A} \quad (2)$$

where γ_{AB} is the interfacial tension, γ_A and γ_B are the surface tensions of the two samples. In this study, the results of interfacial tension values calculated for different systems are given in Table III.

The effect of PP-*g*-MA in PP/ABS blend, $AlCl_3$ in PP/ABS blend, and $AlCl_3$ in PP/PP-*g*-MA/ABS blend was investigated by interfacial tension values. The interfacial tension data demonstrate that the interfacial tension of PP/ABS blend is the highest among all pairs, which shows that there isn't good adhesion between PP and ABS. The interfacial tension value of (PP/ABS/$AlCl_3$)/(PP/ABS) pair has slightly lower than that of PP/ABS system. Although the interface of this blend is also improved during compatibilization process, but severe degradation of phases may be responsible for a slight decrease in interfacial tension. The higher decrease in interfacial tension of (PP/ABS)/PP-*g*-MA pair, suggests the increase of the compatibility of the PP/ABS blends in presence of PP-*g*-MA. According to the result of Table III, the lowest value of interfacial tension is for PP/PP-*g*-MA/ABS/$AlCl_3$ sample, which exhibited highest impact strength. As mentioned, reduction in the interfacial tension in blends shows improvement of adhesion between phases. This means that much improvement of interfacial adhesion is achieved by means of F-C reactions by simultaneous presence of $AlCl_3$ and PP-*g*-MA. The quantitative results of interfacial tensions provided in Table III are in agreement with the observations made by SEM analysis, discussed in previous section.

Table III. Interfacial Tension between Different Materials

Different Pairs	Interfacial Tension (γ_{AB}) (mN/m)
PP/ABS	35.69
(PP/ABS/$AlCl_3$)/(PP/ABS)	20.55
(PP/ABS)/PP-*g*-MA	18.68
(PP/PP-*g*-MA/ABS)/(PP/ABS/$AlCl_3$)	3.11

Conclusions

Reactive compatibilization of PP/ABS blend induced by $AlCl_3$ as a Friedel-Crafts catalyst was studied. The microstructure and performance of the resulting blend systems were evaluated by morphological observations, rheological analysis and mechanical properties. The obtained results led to the following conclusions:

The addition of $AlCl_3$ in different amounts (0.5, 0.7, and 1 wt%) into PP/ABS blend increased the storage modulus along with a decrease in loss tangent as compared with unmod-

ified blend, which was attributed to the increased interfacial interactions between the components in PP/ABS blend. The morphological analysis using SEM further confirmed the improved dispersion of ABS phase domains within the PP matrix. This was ascribed to *in situ* formation of PP-*g*-SAN and/or PP-*g*-ABS copolymer *via* alkylation reactions which act as compatibilizer in the blend system. However, it seems that the degree of improvement was to some extent dependent on the $AlCl_3$ concentration. The results of tensile and Izod impact tests showed that the interfacial adhesion between the phases is not strong enough as the mechanical properties of the resulting blend exhibit only a limited improvements as compared with uncompatibilized blend, but still much lower than those for pure PP. However, when the reactive compatibilization was applied to the PP/ABS blend containing 5 wt% of PP-*g*-MA, a remarkable enhancement was observed in tensile properties and Izod impact toughness of blend systems, compared to neat PP. This was further investigated by SEM, rheological and FTIR analyses and discussed according to chemical reactions occurring in the blend systems containing PP-*g*-MA. The change in interfacial interaction between the components as a result of the presence of PP-*g*-MA and $AlCl_3$ was further verified by contact angle measurements. The increase in impact strength was justified by enhanced interfacial adhesion between the phases, which not only prevents the early decohesion and micro-crack formation at the interfacial region but also triggers efficient stress transfer to the dispersed ABS rubber particles.

References

(1) L. Zhu, X. Xu, and J. Sheng, *J. Polym. Res.*, **18**, 2469 (2011).
(2) S. Hammani, N. Moulai-Mostefa, L. Benyahia, and J. F. Tassin, *J. Polym. Res.*, **19**, 1 (2012).
(3) A. G. Gibson, in *Polypropylene Structure, Blends and Composites*, J. Karger-Kocsis, Ed., Springer Science & Business, London, 1995, vol. 1, pp 71-113.
(4) C. B. Bucknall, *Macromol. Symp.*, **38**, 1 (1990).
(5) A. Van der Wal, J. J. Mulder, H. A. Thijs, and R. J. Gaymans, *Polymer*, **39**, 5467 (1998).
(6) C. B. Bucknall, in *Toughened Plastics*, Springer Science & Business, London, 1997, pp 182-211.
(7) A. Van der Wal, A. J. J. Verheul, and R. J. Gaymans, *Polymer*, **40**, 6057 (1999).
(8) A. Bassani and L. A. Pessan, *J. Appl. Polym. Sci.*, **88**, 1081 (2003).
(9) A. K. Gupta and S. N. Purwar, *J. Appl. Polym. Sci.*, **31**, 535 (1986).
(10) W. Jiang, S. C. Tjong, and R. K. Y. Li, *Polymer*, **41**, 3479 (2000).
(11) Y. Chen and H. Li, *Polym. Eng. Sci.*, **44**, 1509 (2004).
(12) Z. B. Ahmad, M. F. Ashby, and P. W. R. Beaumont, *Scripta Metall.*, **20**, 843 (1986).
(13) Y. Yokoyama and T. Ricco, *Polymer*, **39**, 3675 (1998).
(14) M. M. Mazidi, M. K. R. Aghjeh, and F. Abbasi, *J. Polym. Res.*, **19**, 1 (2012).
(15) A. Van der Wal, R. Nijhof, and R. J. Gaymans, *Polymer*, **40**, 6031 (1999).
(16) L. A. Utracki and B. D. Favis, in *Handbook of Polymer Science and Technology*, N. P. Cheremisinoff, Ed., Marcel Dekker, New York, 1989, vol. 4, pp. 121-201.
(17) L. A. Utracki, *Can. J. Chem. Eng.*, **80**, 1008 (2002).
(18) M. M. Mazidi, M. K. R. Aghjeh, and F. Abbasi, *J. Mater. Sci.*, **47**, 6375 (2012).
(19) M. M. Mazidi, M. K. R. Aghjeh, and F. Abbasi, *J. Appl. Polym. Sci.*, **131**, (2014).
(20) A. C. Patel, R. B. Brahmbhatt, B. Sarawade, and S. Devi, *J. Appl. Polym. Sci.*, **81**, 1731 (2001).
(21) A. C. Patel, R. B. Brahmbhatt, and S. Devi, *J. Appl. Polym. Sci.*, **88**, 72 (2003).
(22) C. K. Kum, Y. T. Sung, Y. S. Kim, H. G. Lee, W. N. Kim, H. S. Lee, and H. G. Yoon, *Macromol. Res.*, **15**, 308 (2007).
(23) H. G. Lee, Y. T. Sung, Y. K. Lee, W. N. Kim, H. G. Yoon, and H. S. Lee, *Macromol. Res.*, **17**, 417 (2009).
(24) T. Y. Kim, D. M. Kim, W. J. Kim, T. H. Lee, and K. S. Suh, *J. Polym. Sci., Part B: Polym. Phys.*, **42**, 2813 (2004).
(25) E. V. Hemelrijck, P. V. Puyvelde, S. Velankar, C. W. Macosko, and P. Moldenaers, *J. Rheol.*, **48**, 143 (2004).
(26) E. V. Hemelrijck, P. V. Puyvelde, S. Velankar, C. W. Macosko, and P. Moldenaers, *J. Rheol.*, **49**, 783 (2005).
(27) M. F. Diaz, S. E. Barbosa, and N. J. Capiati, *J. Polym. Sci., Part B: Polym. Phys.*, **42**, 452 (2004).
(28) R. T. Morrison and R. N. Boyd, in *Organic Chemistry,* Allynand Bacon, New York, 1973, pp 337-371.
(29) B. Reinhard, in *Advanced organic chemistry*, Harcourt/Academic Press, San Diego, 2002, pp 169-212.
(30) W. L. Carrick, *J. Polym. Sci., Part A-1: Polym. Chem.*, **8**, 215 (1970).
(31) W. Barentsen and D. Heikens, *Polymer*, **14**, 579 (1973).
(32) D. Heikens and W. Barentsen, *Polymer*, **18**, 69 (1977).
(33) Y. J. Sun and W. E. Baker, *J. Appl. Polym. Sci.*, **65**, 1385 (1997).
(34) Y. J. Sun, R. J. G. Willemse, T. M. Liu, and W. E. Baker, *Polymer*, **39**, 2201 (1998).
(35) Y. Gao, H. Huang, Z. Yao, D. Shi, Z. Ke, and J. Yin, *J. Polym. Sci., Part B: Polym. Phys.*, **41**, 1837 (2003).
(36) M. F. Diaz, S. E. Barbosa, and N. J. Capiati, *Polymer*, **46**, 6096 (2005).
(37) M. F. Diaz, S. E. Barbosa, and N. J. Capiati, *J. Appl. Polym. Sci.*, **114**, 3081 (2009).
(38) Z. Guo, L. Tong, and Z. Fang, *Polym. Int.*, **54**, 1647 (2005).
(39) R. Kurbanova, R. Mirzaoglu, G. Akovali, Z. M. Rzaev, I. Karatas, and A. Okudan, *J. Appl. Polym. Sci.*, **59**, 235 (1996).
(40) D. Graebling, R. Muller, and J. F. Palierne, *Macromolecules*, **26**, 320 (1993).
(41) D. Graebling, A. Benkira, Y. Gallot, and R. Muller, *Eur. Polym. J.*, **30**, 301 (1994).
(42) Y. Germain, B. Ernst, O. Genelot, and L. Dhamani, *J. Rheol.*, **38**, 681 (1994).
(43) D. O. Hummel, in *Atlas of Polymer and Plastics Analysis*, Vol. 1, Polymers: Structure and Spectra, 1988.
(44) S. Wu, *Polymer Interface and Adhesion*, Marcel Dekker, New York, 1982.